Surface & Coatings Technology 251 (2014) 239–246

Contents lists available at ScienceDirect

Surface & Coatings Technology

journal homepage: www.elsevier.com/locate/surfcoat

Effect of substrate bias on microstructure and properties of Ni–TiN nanocomposite thin films deposited by reactive magnetron co-sputtering

Mukesh Kumar, R. Mitra *

Department of Metallurgical and Materials Engineering, Indian Institute of Technology, Kharagpur 721302, West Bengal, India

ARTICLE INFO

Article history:
Received 10 June 2013
Accepted in revised form 20 April 2014
Available online 25 April 2014

Keywords:
Nanocomposite thin films
Reactive magnetron co-sputtering
Substrate bias
Residual stress
Nano-triboindentation behavior
Electrical resistivity

ABSTRACT

The effect of substrate bias variation on structure and properties of the Ni–TiN nanocomposite thin films deposited on Si (100) substrates by magnetron sputtering has been investigated. Deposition has been carried out by reactive co-sputtering of high purity Ti and Ni targets as RF and DC sources, respectively in an atmosphere with $Ar:N_2 = 1:2$. The microstructures of the as-deposited films have been examined using grazing incidence X-ray diffraction and transmission electron microscopy. It has been observed that with an increase in negative substrate bias from 0 to −80 V, the TiN volume fraction increases from 36 to 50%, whereas the average grain sizes of both Ni (≈10–17 nm) and TiN (≈6–9 nm) decrease. Moreover, the biaxial compressive residual stress as estimated by $\sin^2\psi$ technique scales with negative substrate bias. The surface roughness determined using atomic force microscopy appears to be the least in the nanocomposite film deposited with substrate bias of −60 V. Furthermore, X-ray photoelectron spectroscopy studies have confirmed the formation of oxygen-free stoichiometric TiN in this film. Hardness (≈12.6–16.9 GPa), elastic modulus (≈208–233 GPa) and scratch-resistance determined by nanoindenter, as well as electrical resistivity (≈26–47 μΩ·cm) measured using dc four-probe method, are found to scale with TiN content. An increase in hardness and electrical resistivity with an increase in negative substrate bias is also attributed to a decrease in Ni grain size and an increase in point defect density.

1. Introduction

Nickel-based nanocomposite thin films containing ceramic nanoparticles are considered interesting for use as protective coatings for cylinder liners and piston rods of automobiles as well as for die-casting molds due to their high elastic modulus and hardness along with impressive corrosion resistance [1–4]. Other potential applications are in electrical circuit interconnects and micro-electromechanical systems. Among the commonly studied ceramics, TiN has an advantage due to its metal-like electrical conductivity [5]. The Ni-matrix nanocomposite films can be prepared by either electrodeposition [1–4] or reactive magnetron co-sputtering [6]. Magnetron sputtering of high purity targets under optimized conditions can ensure greater control on composition, finer grain size and higher hardness than the electrodeposition process [6].

For more than two decades, the TiN based nanostructured films have been developed for use in the form of superhard coatings for enhancing the performance of cutting tools. However, these coatings are also known to have very high compressive residual stress and significantly large coefficient of friction, which adversely affect their adhesion with the substrate and wear behavior, respectively [7]. It has been observed that the addition of small amount of Ni to Ti-nitride based coatings is effective not only in restricting grain growth, but also in reducing both compressive residual stress and friction coefficient [7–13]. Furthermore, a study by Chu et al. [14] has shown that the use of the Ni–TiN nanocomposite film as an intermediate layer between the substrate and outer TiN-based superlattice coating is helpful for improving its adhesion. Nickel is preferred as the matrix for the aforementioned nanocomposite film, because both its thermal expansion coefficient and elastic modulus match closely with those of the steel substrate. Another reason for choice of this nanocomposite system is the coexistence of Ni and TiN in thermodynamic equilibrium [15].

In a recent study [6], the Ni–TiN nanocomposite films prepared by reactive magnetron co-sputtering of Ni and Ti targets without application of substrate bias have confirmed the formation of stoichiometric TiN on deposition using $Ar:N_2 = 1:2$. Application of negative substrate bias is known to result in energetic bombardment of the film by positively charged ions of the plasma, thereby leading to an increase in adatom mobility and resputtering of the as-deposited film [16,17]. Therefore, the present study is focused on examining the effect of substrate bias (0 V to −80 V) on growth rate, as well as structure and properties of the Ni–TiN nanocomposite thin films deposited using $Ar:N_2 = 1:2$.

* Corresponding author. Tel.: +91 3222 283292; fax: +91 3222 282280.
E-mail address: rahul@metal.iitkgp.ernet.in (R. Mitra).

http://dx.doi.org/10.1016/j.surfcoat.2014.04.032
0257-8972/

2. Experimental procedure

2.1. Processing

The films were deposited on p-type Si (100) substrates through co-sputtering of Ti and Ni targets (99.99% purity) used as RF and DC sources, respectively in Ar + N_2 atmosphere (purity of 99.999%) inside a chamber for magnetron sputtering system (model KVS-T 4065, Korea Vacuum Tech., Gyeonggi-do, South Korea). The parameters used for deposition are shown in Table 1. Further information regarding processing has been reported elsewhere [6].

2.2. Characterization

The growth rates were determined on the basis of at least 5 measurements of film thickness by a surface profilometer (Dektak150 surface profiler, Veeco Instruments, Plainview, NY, USA) with a diamond stylus having 12.5 μm diameter, following the procedure described in an earlier report [6]. The as-deposited Ni–TiN nanocomposite thin films were further characterized with the help of grazing incidence X-ray diffraction (GIXRD) using Cu K_α radiation (Philips X'Pert PRO Diffractometer, PANalytical, Almelo, The Netherlands). The GIXRD peaks were examined for phase identification, determination of constituent phase volume fractions by Rietveld analysis, as well as estimation of average grain size using the Williamson–Hall relation [18].

The biaxial residual stress in Ni and TiN was measured using the $\sin^2\Psi$ technique [6,19] on a diffractometer in the Bragg–Brentano configuration (Bruker D8 Discover, Germany). For the purpose of stress measurement, the positions of Ni{200} and TiN{200} peaks were obtained for the sample subjected to rotation about the surface normal by three different angles ($\phi = 0°$, 45° or 90°) with respect to a chosen direction. Furthermore, this sample was tilted with respect to the surface normal by angles (ψ) between 0° and 60° with steps of 15° at each value of ϕ. The magnitude of residual lattice strain ($\varepsilon^{(hkl)}{}_{\Psi,\phi}$) at a given tilt angle (ψ) and rotation angle (ϕ) has been calculated using the following relation [19,20]:

$$\varepsilon^{(hkl)}{}_{\Psi,\phi} = \left[\left(d^{(hkl)}{}_{\Psi,\phi} - d_0{}^{(hkl)}\right)/d_0{}^{(hkl)}\right] = \sigma_\phi \sin^2\Psi(1+\nu)/E + \varepsilon^{(hkl)}{}_{0,\phi} \quad (1)$$

$$\text{where } \sigma_\phi = \sigma_{11}\cdot\cos^2\phi + \sigma_{12}\sin^2\phi + \sigma_{22}\cdot\sin^2\phi \quad (2)$$

$$\text{and } \varepsilon^{(hkl)}{}_{0,\phi} = \left(d^{(hkl)}{}_{0,\phi} - d_0{}^{(hkl)}\right)/d_0{}^{(hkl)} = -\nu/E(\sigma_{11}+\sigma_{22}) \quad (3)$$

where $d^{(hkl)}{}_{\Psi,\phi}$ is the spacing between (hkl) planes along the direction defined by angles, Ψ and ϕ, $d^{(hkl)}{}_{0,\phi}$ is the interplanar spacing perpendicular to the specimen surface ($\psi = 0$) in the stressed material, and d_0 is the interplanar spacing in the absence of stress, whereas E is the Young's modulus, and ν is the Poisson's ratio. The experimentally obtained values of $\varepsilon^{(hkl)}{}_{\Psi,\phi}$ were plotted against $\sin^2\Psi$ in order to determine σ_ϕ. The set of three equations obtained for values of $\phi = 0°$, 45°, and 90° were solved to obtain σ_{11}, σ_{22}, and σ_{12}, which in turn were used to calculate the values of principal normal stresses (σ_1 and σ_2). The values of Young's modulus (E) and Poisson's ratio (ν) are $E_{Ni} =$ 210 GPa, $\nu_{Ni} = 0.31$, $E_{TiN} = 440$ GPa, and $\nu_{TiN} = 0.25$.

To analyze stoichiometry of the dispersed phase in the nanocomposite films, X-ray photoelectron spectroscopy (XPS, Model PHI 5000 Versa Probe II, ULVAC-PHI, Inc.) was carried out at the acceleration voltage of 15 kV in a chamber with base vacuum of $\approx 10^{-8}$ Torr. For this study, Al Kα (1.487 keV) radiation with beam size of ≈100 μm^2 was used as the excitation source. The sample surfaces were sputter-cleaned using Ar^+ for 60 s prior to analysis through slow scans.

The microstructures of the as-deposited nanocomposite thin films were examined using a field emission scanning electron microscope (FESEM, Model: Zeiss SUPRA 40, Carl Zeiss SMT GmbH, Oberkochen, Germany) operated at an accelerating voltage of 20 kV. Furthermore, microstructures of electron transparent, cross-section specimens prepared by argon ion-thinning were studied using a transmission electron microscope (TEM, Model: JEM 2100, JEOL Ltd, Tokyo, Japan) operated at an accelerating voltage of 200 kV. The images were recorded on TEM using both bright-field and dark-field imaging modes, whereas the phases were identified by selected area electron diffraction (SAED). Chemical analysis was carried out using the energy dispersive spectroscopy (EDS) facility on FESEM and TEM. Moreover, the surface roughness was measured using an atomic force microscope (AFM) to scan an area of 10 μm × 10 μm on the investigated thin films.

Hardness and Young's modulus of the investigated thin films were evaluated using a nanoindenter (Model TI950 TriboIndenter, Hysitron Inc., Minnesota, MN, USA) having a Berkovich indenter with tip radius of ≈50 nm, that was operated at a loading rate of 0.2 mN/s to a maximum load of 2 mN. The load–displacement plots from at least 25 indents with depths <1/10th of the thickness were averaged for each film. Furthermore, using the same indenter and maximum load as mentioned above, nano-scratch tests were carried out at a lateral speed of 0.5 μm/s to a length of ≈20 μm, and these scratches were imaged in-situ using an AFM attached to the nanoindenter.

Electrical resistivity measurements were carried out on the investigated thin films grown using the conditions mentioned in Table 1 on Si (100) wafers with a SiO_2 scale grown on its surface by exposure in air at 1000 °C for 1 h in a horizontal tube furnace. The electrical resistivity of the nanocomposite thin film was measured by the Van der Pauw four point probe method (Keithley Model 220 Programmable Current Source and Model 2182 Nano-voltmeter, Cleveland, OH, USA), as described in an earlier report [6].

Table 1
Process parameters used for the deposition by reactive co-magnetron sputtering of Ni and Ti targets.

Process parameters	Values
Base pressure	2.0×10^{-6} Torr
Working pressure	20 mTorr
Ar:N_2	1:2
Ti RF power	300 W
Ni DC power	50 W
Substrate temperature	Ambient
Substrate bias	0, −20, −40, −60 and −80 V
Substrate rotation speed	25 rpm
Substrate to target distance	120 mm
Duration of deposition	1 h

3. Results and discussion

3.1. Rate of film growth

The average thickness of the as-deposited films has been found to vary from ≈350 nm to 500 nm, depending upon their growth rates. Plots depicting the variation of growth rates of the Ni, TiN and Ni–TiN nanocomposite thin films against negative substrate bias used for deposition are shown in Fig. 1. The results in this figure show that at a given substrate bias, the sputter yield of Ni target is much higher than that of Ti. Therefore, the Ni target power has been kept as 1/6th of that used for Ti in order to have dispersion of a suitable volume fraction of TiN. The growth rate of Ni matrix is also reduced in order to achieve higher film density. Furthermore, the growth rate of the Ni film has been found to decrease with an increase in negative substrate bias voltage (Fig. 1). This observation can be attributed primarily to re-sputtering of adatoms from the as-deposited film as well as greater amount of densification caused by the energetic bombardment of Ar^+ ions.

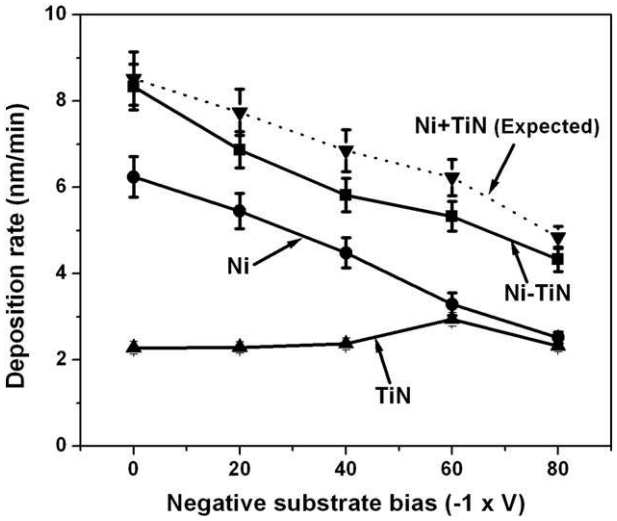

Fig. 1. Plots depicting the variation of film growth rate with applied substrate bias.

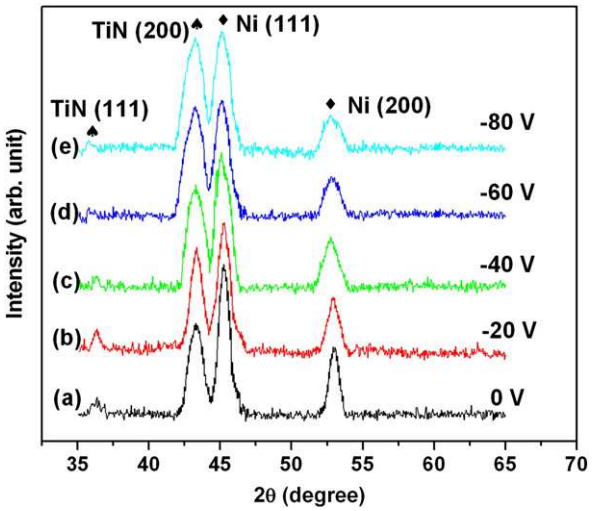

Fig. 2. GIXRD patterns obtained from the Ni–TiN nanocomposite thin films deposited using substrate bias of: (a) 0 V, (b) −20 V (c) −40 V, (d) −60 V, and (e) −80 V.

Interestingly, the growth rate of TiN film is increased marginally with an increase in the substrate bias from 0 to −60 V, whereas it is decreased on further increase to −80 V, similar to the behavior reported by Jiang et al. [21]. Due to its high reactivity, the sputtered Ti atoms are expected to be partially ionized by collisions with positively charged ions in the plasma. The ion current density is expected to increase up to negative substrate bias of −60 V, and then reach saturation in a manner similar to that reported by Jiang et al. Furthermore, the kinetics of TiN formation by in-situ reaction between neutral or ionized Ti and chemisorbed N_2^+ is enhanced due to an increase in adatom mobility with substrate bias, which in turn lowers the resputtering rate of the unreacted species. However, on increase in the substrate bias till −80 V, energetic bombardment of Ar^+ is probably high enough to raise the resputtering rate of unreacted Ti and N_2^+ to such an extent that the apparent growth rate of TiN is reduced.

The results in Fig. 1 show that deposition rates of the Ni–TiN nanocomposite film as predicted by addition of the individual growth rates of Ni and TiN films are found to exceed the experimentally observed values, except for the substrate bias voltages of 0 V and −80 V. The presence of Ni adatoms is expected to act as a barrier for the reaction between Ti and N_2^+, and thereby retard the reaction kinetics. Reduction in the rate of formation of TiN could cause an increase in the desorption rate of Ti and N_2^+, which could lower the overall growth rate of the nanocomposite film.

3.2. Microstructure

3.2.1. Phase identification and morphology

The results of GIXRD analysis of the Ni–TiN nanocomposite thin films deposited using different substrate bias voltages as shown in Fig. 2(a) through (e) reveal the presence of Ni and TiN peaks. A typical FESEM micrograph depicting the granular microstructure of the nanocomposite thin film deposited at substrate bias of −60 V is shown in Fig. 3. Furthermore, the Ni:Ti ratios as determined by bulk EDS analysis as shown in Table 2, indicates that the atomic fraction of Ti is increased at the expense of Ni with an increase in negative substrate bias voltage. Typical bright-field and dark-field TEM micrographs depicting the cross-sectional microstructure of the nanocomposite Ni–TiN thin films deposited at the substrate bias of −60 V are shown in Fig. 4(a) and (b), respectively, whereas the corresponding SAED pattern confirming the presence of Ni and TiN is shown in Fig. 4(c). The TEM dark-field image in Fig. 4(b) shows the presence of equiaxed, nanometric grains. The average grain sizes of Ni and TiN measured from several dark-field images are shown in Table 3. The lattice image depicting the microstructure of the nanocomposite film grown with substrate bias of 0 V, as shown in Fig. 5, indicates that the TiN grains are faceted with the Ni–TiN interfaces being atomically abrupt.

3.2.2. Volume fraction of TiN

Examination of the GIXRD patterns shown in Fig. 1 indicates that with an increase in substrate bias from 0 V to −80 V, the intensities of the peaks representing TiN are increased, while those belonging to Ni are lowered. Rietveld analysis of the XRD peaks have shown the volume fractions of TiN to increase from 36% to 50% with an increase in the substrate bias from 0 V to −80 V, as shown in Table 2. The increase in the TiN volume fraction at the expense of Ni can be attributed to a sharper fall in the growth rate of Ni than that of TiN with the increase in negative substrate bias, as shown in Fig. 1.

Comparison of the Ni:Ti ratios calculated on the basis of TiN volume fractions obtained through Rietveld analysis agrees closely with those estimated directly by EDS analyses. The results in Table 2 also show that the Ni:TiN ratios obtained from the individual growth rates of Ni and TiN are significantly higher than those derived from the results of Rietveld analyses. The reason for this discrepancy can be attributed to retardation in the rate of TiN formation due to the presence of Ni adatoms, as discussed in Section 3.1.

3.2.3. Grain size

The average grain sizes of Ni and TiN in the nanocomposite thin films grown at different substrate bias voltages, as determined by analyzing the GIXRD peaks using the Williamson–Hall relation, are shown in

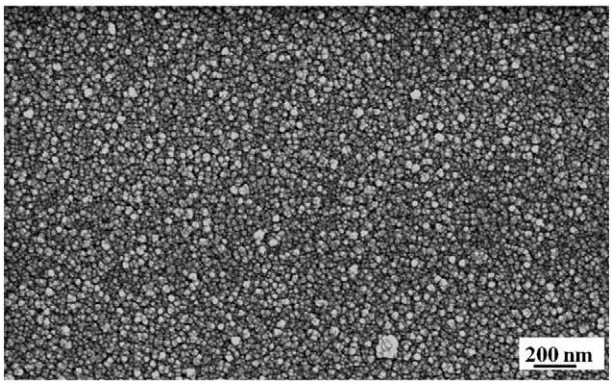

Fig. 3. FESEM micrograph depicting the microstructure of the Ni–TiN nanocomposite films deposited with the substrate bias of −60 V.

Table 2
The ratios of Ni:Ti and Ni:TiN obtained on the basis of EDS and Rietveld analyses.

Substrate bias (V)	Ni:Ti ratio on the basis of:		Ni:TiN ratio on the basis of:	
	EDS analysis	Rietveld analysis	Rietveld analysis	Growth rate of Ni and TiN films
0	2.8:1	2.7:1	64:36	73:27
−20	2.4:1	2.4:1	61:39	70:30
−40	2.1:1	2.0:1	57:43	65:35
−60	1.7:1	1.7:1	52:48	53:47
−80	1.6:1	1.5:1	50:50	52:48

Table 3. The results in this table show an excellent agreement between the grain sizes obtained by XRD and dark-field TEM analyses. Moreover, with an increase in the negative substrate bias from 0 V to −80 V, the average grain sizes of Ni and TiN are decreased by 41% and 34%, respectively. Due to energetic bombardment of the film by Ar^+ ions with an increase in the negative substrate bias, the distribution of nucleating islands is expected to be more uniform [16,17], thereby reducing the average grain size as confirmed by the results presented in Table 3. Moreover, the increase in the volume fraction of TiN with the increase in negative substrate bias, as discussed above, is also expected to restrict the matrix grain growth.

3.3. Residual stress

The values of biaxial residual stress obtained for Ni and TiN as shown in Table 4 are found to be compressive in character. Furthermore, the magnitude of this stress is found to increase with an increase in the negative substrate bias, and the amount of stress in the TiN phase exceeds that in Ni. The presence of compressive residual stress in both Ni and TiN as well as its increase with substrate bias, as shown in this table, may be attributed to atomic shot-peening effect [22] and formation of Frenkel pairs [20,23] caused by energetic bombardment of Ar^+ ions. As the Frenkel pairs are created in the films by bombardment of Ar^+ ions, their concentration is expected to scale with the negative substrate bias.

3.4. Surface roughness

The plots of surface roughness obtained by AFM studies on Ni, TiN and Ni–TiN nanocomposite thin films against the negative substrate bias used for deposition are shown in Fig. 6. The decrease in surface roughness with an increase in the applied substrate bias till −60 V as shown in this figure may be attributed to the increase in surface density by closure of pores through rearrangement of adatoms [16,21], which is possible due to their enhanced mobility.

It is interesting to note that for deposition with a specified substrate bias, the surface roughness value obtained for the pure Ni film is much higher than that of either Ni–TiN nanocomposite or TiN film. Therefore a decrease in Ni content of the film with increasing substrate bias could be one of the reasons for a decrease in surface roughness. The sharp rise in surface roughness with an increase in negative substrate bias from −60 V to −80 V, as shown in Fig. 6, may be attributed to the formation of surface defects due to energetic bombardment by Ar^+ ions [21].

3.5. Stoichiometry of TiN

The complete XPS spectrum of the Ni–TiN nanocomposite films has shown the peaks of Ti, C, O and N [6]. The surface-based impurities such as C and O introduced by contact of the film with air could be partially removed by sputtering with Ar^+. The XPS spectra showing the peaks of Ti 2p, N 1s and Ni 2p obtained from the investigated nanocomposite thin films using slow scan are shown in Fig. 7(a), (b) and (c), respectively. As shown in Fig. 7(a), a shift in the values of BE for the XPS peaks representing Ti ($2p_{3/2}$) from 455.4 eV to 454.9 eV is observed, as the substrate bias is changed from 0 V to −80 V. Similarly, the BE of N (1s) peak is decreased from 397.8 eV to 396.7 eV for a similar change in the substrate bias [Fig. 7(b)]. However, as expected, the XPS peaks representing Ni [Fig. 7(c)] in elemental form at BE = 852.5 eV ($2p_{3/2}$) and 869.6 eV ($2p_{1/2}$) are sharper than those representing Ti and N.

The systematic variation in the position of the XPS peaks of Ti and N with change in the substrate bias voltage as shown in Fig. 7(a) and (b) may be attributed to the difference in both oxygen content and stoichiometry (Ti/N ratio) of TiO_yN_x. For the stoichiometric TiN with 0 at.% O, the XPS peaks representing Ti ($2p_{3/2}$), Ti ($2p_{1/2}$), and N (1s) are reported to be located at 455.03 ± 0.05 eV, 460.85 ± 0.05 eV, and 397.11 ± 0.04 eV, respectively [24]. These values of BE are found for the XPS peaks from the nanocomposite film deposited at substrate bias of −60 V. Based on the results in the literature [24–26], it is inferred that in the nanocomposite films grown with substrate bias between 0 and −40 V, the value of y is >0 in TiO_yN_x, whereas y = 0 in the film deposited using substrate bias = −60 V and −80 V.

It has been shown by Jiang et al. [21] that the use of the optimum substrate bias causes the formation of TiN film with stoichiometric composition, such that the formation of surface oxides during subsequent exposure to atmosphere is restricted. The reduced tendency for oxidation of such films may be ascribed to smooth surfaces with a minimum amount of defects observed on growth with optimum substrate bias, which is −60 V in this study. Furthermore, the XPS peak positions representing Ti ($2p_{3/2}$), Ti ($2p_{1/2}$), and N (1s) for the film deposited with the substrate bias of −80 V are suggestive of sub-stoichiometric composition (Ti/N > 1), which may be attributed to increased desorption rate of N_2^+ caused by energetic bombardment of Ar^+ ions during deposition.

3.6. Nanoindentation hardness and elastic modulus

Plots depicting the variation of Young's modulus and hardness found by nanoindentation with TiN volume fraction are shown in Fig. 8(a) and (b), respectively. In these plots, the rule of mixtures (ROM) predictions on the basis of the results obtained for pure Ni and TiN films are also shown for the purpose of comparison. Examination of the results in these figures indicates that hardness and Young's moduli lie in the range of 12.6–16.9 GPa and 207.4–233.4 GPa, respectively, which agree reasonably with the results reported in earlier studies [6,7].

Whereas the Young's modulus obtained by nanoindentation on the nanocomposite thin film with a given volume fraction of TiN is found to be nearly equal to that predicted by ROM [Fig. 8(a)], the corresponding hardness value is found to be higher [Fig. 8(b)]. This observation regarding hardness is similar to that reported for multilayered nanocomposite films [27] and may be attributed to higher hardness of the Ni matrix of the nanocomposite than that of the unreinforced Ni film. Higher hardness of matrix in the nanocomposite film is expected to be due to finer grain size than that in the pure Ni films, as well as image forces experienced by dislocations at Ni–TiN interfaces [6]. The increase in hardness with TiN volume fraction can also be attributed partly to the increase in point defect density with negative substrate bias, as reported in earlier studies [20,23].

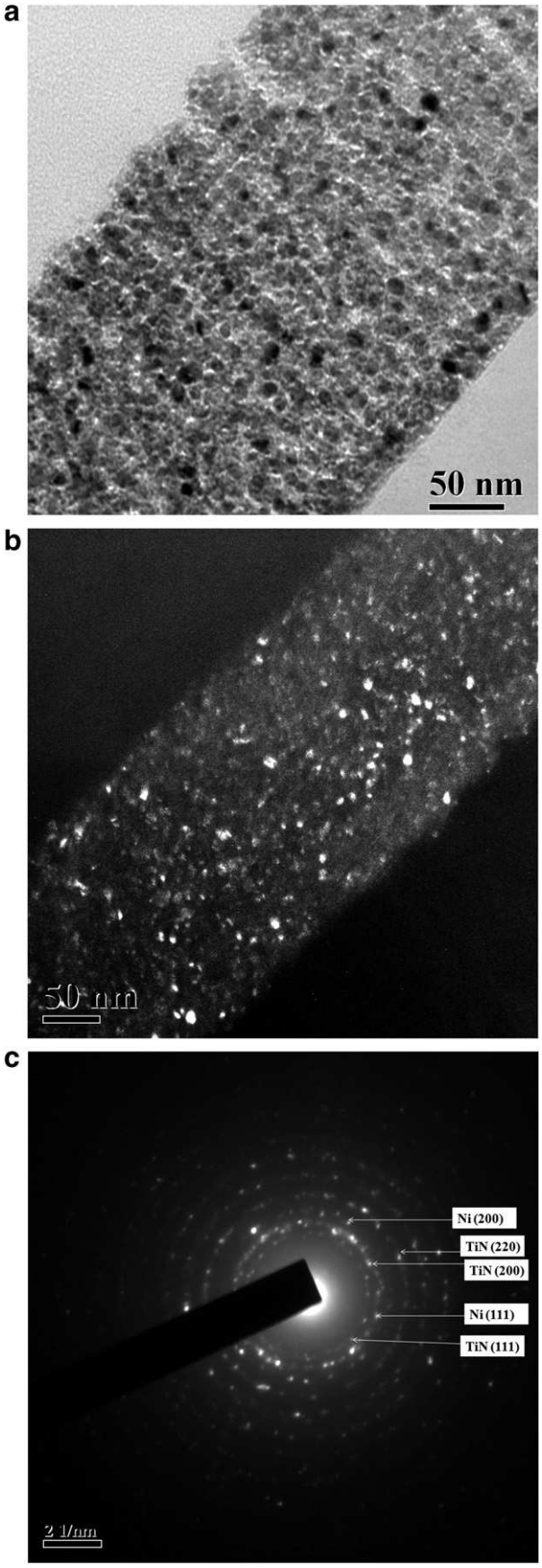

Fig. 4. Results of TEM studies on the cross-section microstructure of the Ni–TiN nanocomposite thin film sample deposited at the substrate bias of −60 V: (a) bright field image, (b) dark field image, and (c) the corresponding SAED pattern.

Table 3
Mean grain sizes found by XRD analyses for Ni and TiN in the nanocomposite thin films deposited at different negative substrate biases. The grain size measured by TEM dark field studies is also shown for comparison.

Substrate bias (V)	Grain size measured by XRD (nm)		Grain size measured by TEM (nm)	
	Ni	TiN	Ni	TiN
0	17	9	18 ± 1	9 ± 1
−20	16	9	15 ± 2	8 ± 1
−40	14	8	13 ± 1	8 ± 1
−60	11	7	12 ± 1	7 ± 1
−80	10	6	10 ± 1	6 ± 1

3.7. Nano-tribological properties

A typical AFM image depicting the scratch formed by the Berkovich indenter in the nanocomposite thin film deposited at substrate bias of −60 V as shown in Fig. 9 shows formation of hillocks on either side of scratch. This observation confirms that plowing mechanism involving plastic deformation is effective in displacing material from inside the trough. The average values of width (W) and depth (D) obtained from the results of 5–6 measurements carried out on scratches by AFM are plotted against TiN volume fraction in Fig. 10. The linear fit in this figure with $R^2 > 0.9$ indicates that scratch resistance is directly proportional to TiN content of the nanocomposite film.

It has been conclusively shown by Tsui et al. [28] that the resistance to plastic deformation by a rigid spherical indenter is proportional to the value of H^3/E^{*2}, where H is the hardness and E^* is the biaxial Young's modulus $= E / (1 - \nu^2)$, with E and ν being Young's modulus and Poisson's ratio, respectively. The average scratch-width (W) has been plotted against H and H^3/E^{*2} obtained for the investigated nanocomposite thin films in Fig. 11(a) and (b), respectively. The equations for the best-fit lines in these plots are:

$$W = 629.2 - 15 \cdot H \qquad \left(R^2 = 0.85\right) \tag{4}$$

$$W = 516.3 - 1903.5 \cdot \left(H^3/E^*\right)^2 \qquad \left(R^2 = 0.90\right). \tag{5}$$

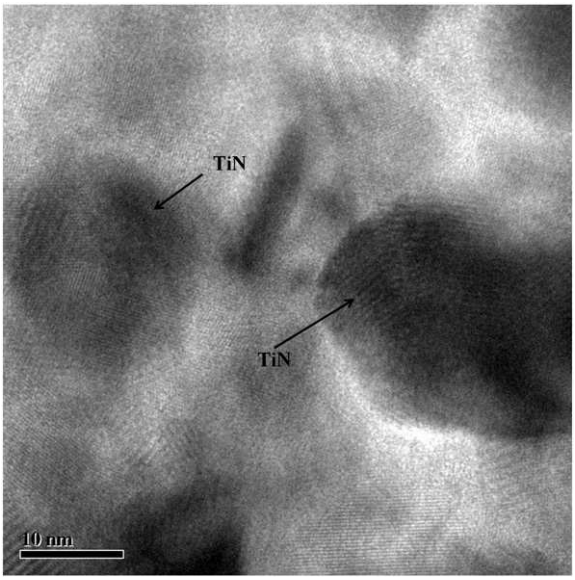

Fig. 5. Atomic resolution image depicting the microstructure of Ni–TiN nanocomposite thin films deposited at the substrate bias of 0 V.

Table 4
Residual stresses in Ni and TiN as measured by XRD analyses.

Substrate bias (V)	Ni {200} peak		TiN {200} peak	
	σ_1 (GPa)	σ_2 (GPa)	σ_1 (GPa)	σ_2 (GPa)
0	−1.5	−0.5	−2.1	−1.0
−20	−1.7	−0.8	−2.3	−1.1
−40	−1.9	−1.1	−2.6	−1.3
−60	−2.2	−1.3	−2.8	−1.6
−80	−2.5	−1.5	−3.0	−1.8

Based on the R^2 values for the above linear relations, it is appropriate to infer that the scratch resistance is more fundamentally related to the parameter, H^3/E^{*2} than to H.

The coefficient of friction (COF) is found to decrease with the increase in substrate bias, as shown in the plots depicted in Fig. 12. As reported in some of the previous studies [29,30], the force of friction depends on the combined effects of surface roughness, adhesive character of contact and volume of displaced material. Both adhesive character of contact and volume of displaced material are expected to increase with increasing Ni content and decreasing hardness of the film. Therefore, the highest value of COF is found for the films grown with substrate bias of 0 V. Interestingly, the lowest COF has been recorded for the film grown using substrate bias of −80 V in spite of its high surface roughness. This observation indicates that lowering of both adhesive interaction and volume of displaced material due to higher hardness of the film grown with substrate bias of −80 V could have greater influence on the COF than surface roughness.

3.8. Electrical resistivity

The values of electrical resistivity are found to increase linearly with TiN volume fraction, as shown in Fig. 13. The results of resistivity measurements carried out on the nanocomposite thin film without the application of any substrate bias at different Ar:N_2 ratios [6] are also shown for the purpose of comparison. It is clear that the slope of the best fit line for the plot of electrical resistivity against TiN content for the films deposited with negative substrate bias is much greater than that for the data representing the film processed without substrate bias. Such a sharp difference in the electrical behavior of the film subjected to substrate bias during deposition may be attributed to higher point defect density and finer grain size of the Ni matrix, compared to those in the films grown without substrate bias.

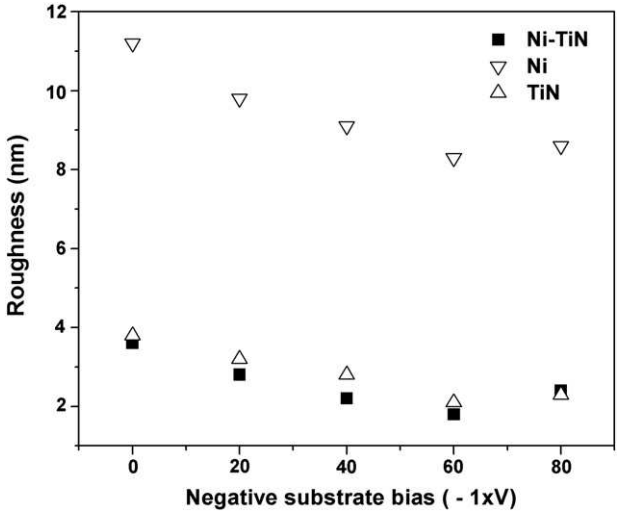

Fig. 6. Plots depicting the variation of surface roughness as measured by AFM, with negative substrate bias used for deposition for the thin films of Ni, TiN and Ni–TiN nanocomposite.

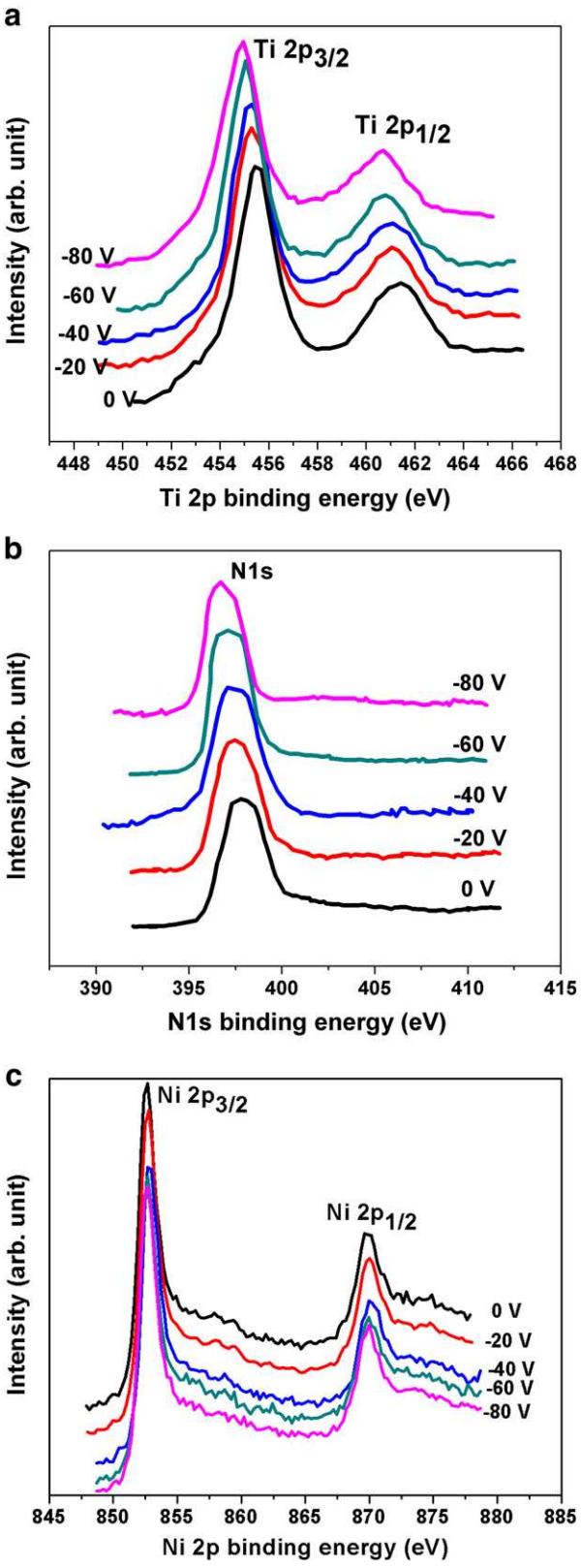

Fig. 7. The parts of XPS spectrum recorded through slow scan after sputtering with Ar^+ ions for 60 s showing: (a) Ti ($2p_{3/2}$) and Ti ($2p_{1/2}$) peaks, (b) N (1s) peaks, and (c) Ni ($2p_{3/2}$) and Ni ($2p_{1/2}$) peaks.

4. Conclusions

The relationship between process parameters, microstructure and properties of the Ni–TiN nanocomposite thin films prepared by

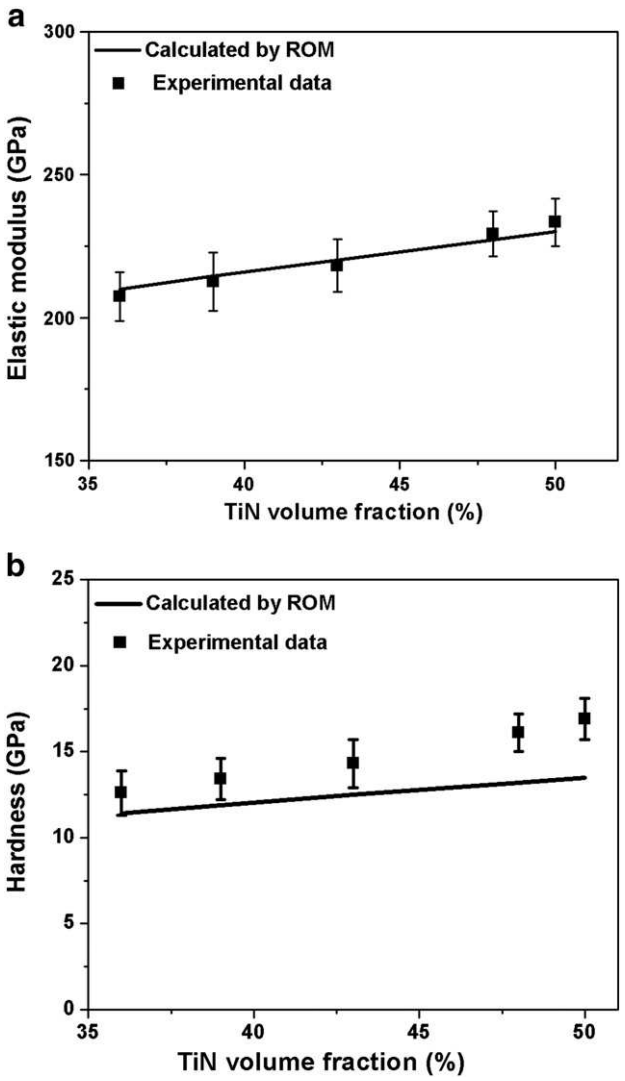

Fig. 8. Plots showing the variation of: (a) Young's modulus and (b) hardness with TiN volume fraction, for the nanocomposite thin films deposited at different negative substrate biases.

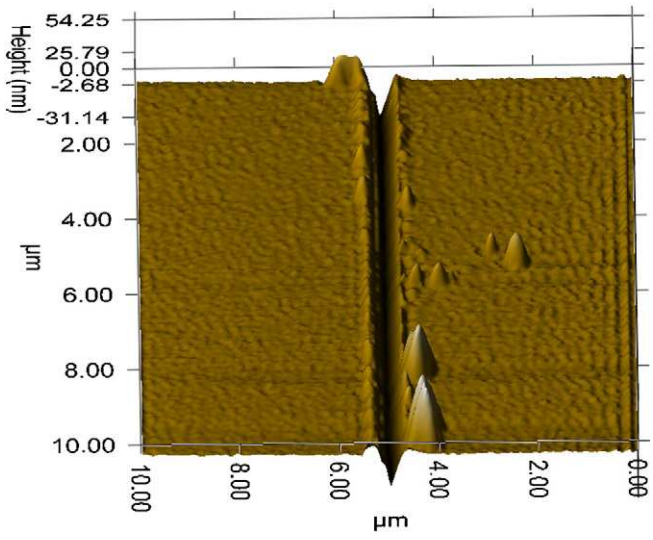

Fig. 9. Typical AFM image depicting the scratch on the surface of Ni–TiN nanocomposite thin films deposited at substrate bias of −60 V.

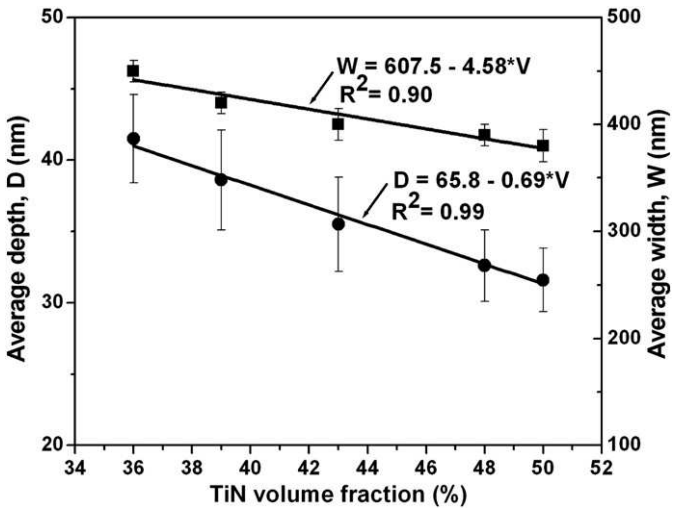

Fig. 10. Plots depicting the variation of depth (D) and width (W) of the scratch introduced by the Berkovich indenter with TiN volume fraction.

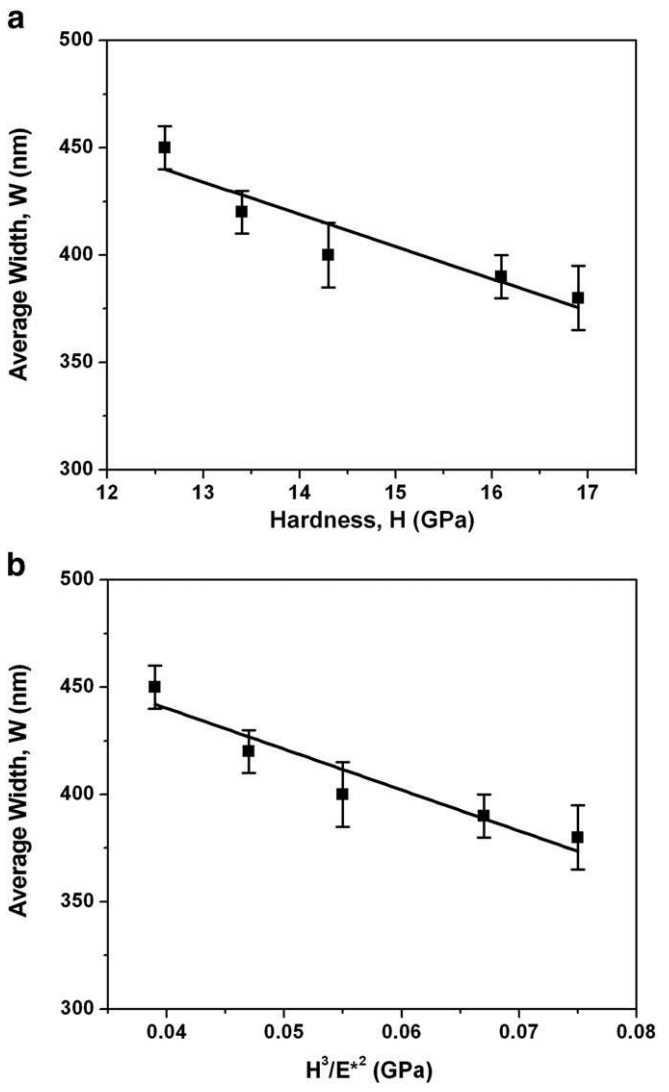

Fig. 11. Plots depicting the variation of width (W) of the scratch with: (a) hardness (H) and (b) H^3/E^{*2} [where $E^* = E / (1 - \nu^2)$].

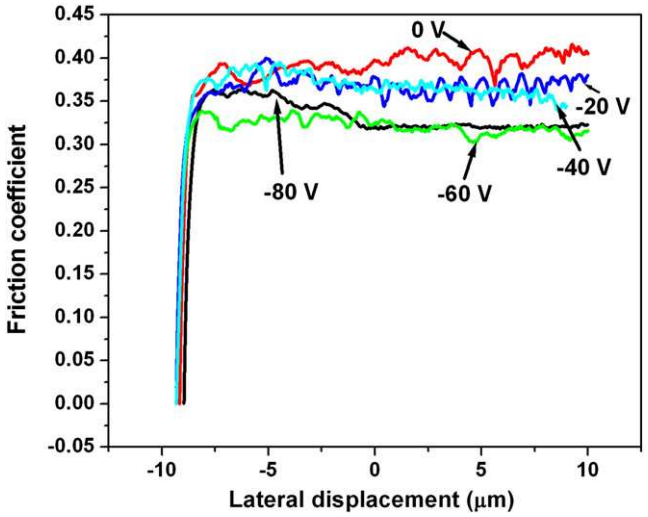

Fig. 12. Variation of coefficient of friction (COF) with lateral displacement of indenter operated at constant load of 2 mN.

magnetron co-sputtering of Ni and Ti targets in Ar + N_2 atmosphere at substrate bias voltages between 0 V and −80 V have been investigated. The following conclusions are drawn from the present study:

(i) It has been shown that the Ni–TiN nanocomposite thin films with volume fractions of TiN varying from 36% to 50% can be prepared by changing the negative substrate bias from 0 V to −80 V. Increase in the TiN volume fraction with increasing negative substrate bias is attributed to preferential resputtering of Ni.

(ii) Increase in the negative substrate bias during deposition leads to reduction in growth rate of the nanocomposite thin films, while surface roughness is also reduced till the negative substrate bias is increased to −60 V.

(iii) Using XRD and TEM studies, the average grain sizes of Ni and TiN have been found to be in the range of ≈10.2–17.6 nm and ≈6.0–9.0 nm, respectively.

(iv) Both hardness and elastic modulus of the films found by nanoindentation are found to increase with the increase in volume fraction of TiN, whereas the scratch resistance scales closely with both TiN content and resistance to plastic deformation.

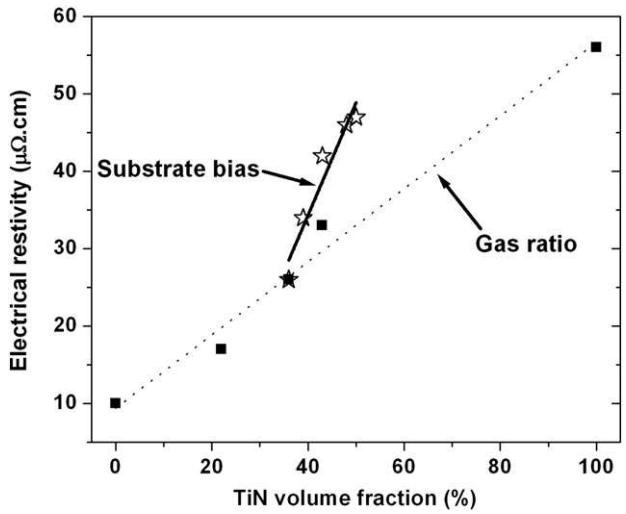

Fig. 13. Plot depicting the variation of electrical resistivity (ρ) with TiN volume fraction of the nanocomposite thin films grown at different substrate bias voltages. The results obtained for the films grown at 0 V substrate bias with different Ar:N_2 ratios (fitted to dotted line) are shown for comparison.

(v) The electrical resistivity is found to increase with the increase in TiN volume fraction and point defect density, as well as with the decrease in the matrix grain size.

Conflict of interest

There is no conflict.

Acknowledgments

The authors express their gratitude to Mr. Dilip Kumar Chakraborty, Department of Metallurgical and Materials Engineering, for the technical assistance with processing, as well as to Mr. Mithun Das, Mr. Tapas Paul and Mr. Ranadhir Bosu, Central Research Facility for the assistance with characterization. The help received from Prof. S.K. Srivastava, Department of Physics for XPS studies is also gratefully acknowledged.

References

[1] C.T.J. Low, R.G.A. Wills, F.C. Walsh, Surf. Coat. Technol. 201 (2006) 371–383.
[2] L. Benea, P.L. Bonora, A. Borello, S. Martelli, Mater. Corr.Werr. Korr. 53 (1) (2002) 23–29.
[3] F. Xia, M. Wu, F. Wang, Z. Jia, A. Wang, Curr. Appl. Phys. 9 (2009) 44–47.
[4] Z. Xu-bei, C. Chao, Z. Guo-qu, Z. Zhao, L. Jin-feng, Trans. Nonferrous Met. Soc. China 21 (2011) 2216–2224.
[5] R. Mientus, K. Ellmer, Surf. Coat. Technol. 116–119 (1999) 1093–1101.
[6] M. Kumar, S. Mishra, R. Mitra, Surf. Coat. Technol. 228 (2013) 100–114.
[7] X. Chu, M.S. Wong, W.D. Sproul, S.A. Barnett, Surf. Coat. Technol. 57 (1) (1993) 13–18.
[8] X. Chu, M.S. Wong, W.D. Sproul, S.A. Barnett, Surf. Coat. Tech. 61 (1993) 251–256.
[9] M. Misina, J. Musil, S. Kadlec, Surf. Coat. Technol. 110 (1998) 168–172.
[10] S. Zhang, D. Sun, Y. Fu, Y.T. Pei, J.T.M.D. Hosson, Surf. Coat. Technol. 200 (2005) 1530–1534.
[11] Z.G. Li, S. Miyake, M. Kumagai, H. Saito, Y. Muramatsu, Surf. Coat. Technol. 183 (2004) 62–68.
[12] A. Akbari, C. Templier, M.F. Beaufort, D. Eyidi, J.P. Riviere, Surf. Coat. Technol. 206 (5) (2011) 972–975.
[13] J. Musil, J. Vlcek, Surf. Coat. Technol. 142–144 (2001) 557–566.
[14] X. Chu, M.S. Wong, W.D. Sproul, S.A. Barnett, Surf. Coat. Technol. 61 (1993) 251–256.
[15] I. Barin, Thermochemical Data of Pure Substances, vols. 1 and 2, VCH, Weinheim, Germany, 1989. (pp. 1229, 1230, 1689).
[16] K.L. Chopra, Thin Film Phenomena, Mc-Graw Hill Book Company, New York, 1969. 137.
[17] R. Mitra, R.A. Hoffman, A. Madan, J. Mater. Res. 16 (7) (2001) 2064–2076.
[18] G.K. Williamson, W.H. Hall, Acta Metall. 1 (1) (1953) 22–31.
[19] B.D. Cullity, Elements of X-ray Diffraction, Second edition Addison-Wesley Publishing Company, Inc., Reading, MA, 1978. (Chap. 9, pp. 281, 447).
[20] Y.H. Jin, D.Y. Chung, J. Korean Ceram. Soc. 48 (5) (2011) 458–462.
[21] N. Jiang, H.J. Zhang, S.N. Bao, Y.G. Shen, Z.F. Zhou, Physica B 352 (2004) 118–126.
[22] J.A. Thornton, D.W. Hoffman, J. Vac. Sci. Technol. 14 (1977) 164–168.
[23] M. Wen, Q.N. Meng, W.X. Yu, W.T. Zheng, S.X. Mao, M.Z. Hua, Surf. Coat. Technol. 205 (2010) 1953–1961.
[24] D. Jaeger, J. Patscheider, J. Electron Spectrosc. Relat. Phenom. 185 (2012) 523–534.
[25] I. Bertoti, M. Mohai, J.L. Sullivan, S.O. Saied, Appl. Surf. Sci. 84 (4) (1995) 357–371.
[26] M. Wolf, J.W. Schultze, H.-H. Strehblow, Surf. Interface Anal. 17 (1991) 726–736.
[27] B.M. Clemens, H. Kung, S.A. Barnett, MRS Bull. 24 (2) (1999) 20–26.
[28] T.Y. Tsui, G.M. Pharr, W.C. Oliver, C.S. Bhatia, R.L. White, S. Anders, A. Anders, I.G. Brown, , (Materials Research Society, Pittsburgh, PA) Mater. Res. Soc. Symp. Proc. 383 (1995) 447. http://dx.doi.org/10.1557/PROC-383-447 (Published online by Cambridge University Press, 15 February, 2011).
[29] Y. Chen, S.R. Bakshi, Surf. Coat. Technol. 204 (2010) 2709–2715.
[30] X.M. Liu, Z.L. Liu, Y.G. Wei, Tribol. Lett. 46 (2012) 167–178.